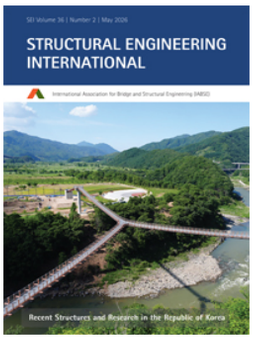

Taylor & Francis
Taylor & Francis Group

Structural Engineering International

ISSN: 1016-8664 (Print) 1683-0350 (Online) Journal homepage: www.tandfonline.com/journals/tsei20

Flexure and Shear Stop Criteria for Proof Load Testing of Reinforced Concrete Slab Bridges

Gabriela Zarate Garnica, Fengqiao Zhang Dr., Yuguang Yang Dr., Max A. H. Hendriks Prof. Dr. & Eva O. L. Lantsoght Prof. Dr.

To cite this article: Gabriela Zarate Garnica, Fengqiao Zhang Dr., Yuguang Yang Dr., Max A. H. Hendriks Prof. Dr. & Eva O. L. Lantsoght Prof. Dr. (05 May 2026): Flexure and Shear Stop Criteria for Proof Load Testing of Reinforced Concrete Slab Bridges, Structural Engineering International, DOI: 10.1080/10168664.2026.2639993

To link to this article: https://doi.org/10.1080/10168664.2026.2639993

Published online: 05 May 2026.

Flexure and Shear Stop Criteria for Proof Load Testing of Reinforced Concrete Slab Bridges

Gabriela Zarate Garnica, Concrete Structures, Department of Engineering Structures, Civil Engineering and Geosciences, Delft University of Technology, Delft, the Netherlands; **Fengqiao Zhang**, Dr., Concrete Structures, Department of Engineering Structures, Civil Engineering and Geosciences, Delft University of Technology, Delft, the Netherlands; **Yuguang Yang**, Dr., Concrete Structures, Department of Engineering Structures, Civil Engineering and Geosciences, Delft University of Technology, Delft, the Netherlands; **Max A. H. Hendriks**, Prof. Dr., Concrete Structures, Department of Engineering Structures, Civil Engineering and Geosciences, Delft University of Technology, Delft, the Netherlands NTNU, Trondheim, Norway; **Eva O. L. Lantsoght**, Prof. Dr., Concrete Structures, Department of Engineering Structures, Civil Engineering and Geosciences, Delft University of Technology, Delft, the Netherlands Decanato de Investigación, Universidad San Francisco de Quito, Diego de Robles y Pampite s/n, Campus Cumbaya, Quito EC 170157, Ecuador. Contact: elantsoght@usfq.edu.ec

DOI: 10.1080/10168664.2026.2639993

Abstract

Proof load testing on bridges requires high magnitude loads. Stop criteria are used to avoid irreversible damage or failure during proof load testing. These stop criteria are thresholds to measurable parameters during the test. After reaching a stop criterion, the proof load test needs to be terminated. While in the past, stop criteria have been identified as a single level, this research proposes to use a traffic light system for stop criteria: green light (related to the serviceability limit state), yellow light (as an intermediate level) and red light (further testing is not permitted). The green light relates to the development of cracking, whereas the yellow and red light relate to the failure modes of flexure and shear. To develop stop criteria for the brittle failure mode of shear, thresholds are derived from mechanical models, based on strain measurements and crack widths, as well as using acoustic emission measurements. To validate the stop criteria, three series of experiments are analyzed: reinforced concrete slab strips, straight slabs, and skewed slabs. While field validation of the traffic light system is pending, the developed tool is a step forward to safely test concrete bridges without shear reinforcement.

Keywords: Bridge assessment; Damage indicators; Experiments; Mechanical models; Proof load testing.

Introduction

As a large number of bridges in various parts of the world are ageing, the need for the assessment of existing bridges is increasing.[1–15] In the Netherlands, for example, a significant percentage of the existing bridge stock dates back to the 1960s and 1970s. These bridges were designed using capacity models that differ from the models used in our current codes. As a result, upon an initial assessment, a large number of existing reinforced concrete solid slab bridges in the Netherlands are found to be shear-critical and require further analysis. Assessment of reinforced concrete solid slab bridges is carried out using Levels of Approximation[13,16–18] for Assessment, also known as Levels of Assessment.[19] The first level is the so-called "Quick Scan", which uses hand calculations programmed into a spreadsheet for a quick selection of the critical bridges and sections. The reader may be interested to learn that this approach is centralized, after different spreadsheet-based approaches using different assumptions were found to lead to large differences in assessment outcomes, due to the so-called engineering-effect. The second level uses linear finite element models to better evaluate the load effect, while keeping the capacity as determined in level 1. The third level can use either probabilistic models or nonlinear finite element models, which require significant amounts of input data. The fourth and final level of assessment allows for the use of bridge proof load testing to demonstrate directly that the tested bridge fulfills the safety requirements.

Proof load testing involves the application of the code-prescribed live loads to the bridge, or a load that results in the same sectional load effect as the considered load combination from the governing code. As such, high magnitude loads are applied, and the risks associated with testing become large. Therefore, stop criteria need to be determined. Stop criteria are thresholds to the measured parameters. When these thresholds are reached or exceeded, further loading is not permitted, as further loading can result in irreversible damage or even collapse of the element or bridge. Currently used stop criteria include the stop criteria as used in the German guideline[20] and the acceptance criteria from ACI 437.2-22.[21] These stop and acceptance criteria are, for example, based on a maximum predefined crack width, such as 0.3 mm, or a maximum deflection. However, since these are not based on theoretical sectional models, their performance for shear-critical tests is low.[22–24] As compared to the previous version ACI 437.2M-13[25], ACI 437.2-22 explicitly includes shear-critical members.

Considering the large need for the assessment of existing reinforced concrete solid slab bridges that may be shear-critical, and the promising approach of proof load testing, the main research gap can be identified as follows: to be able to carry out proof load testing for shear, stop criteria for shear, that are based on the

shear mechanics, need to be identified. This requires finding indicators that signal shear distress, before a brittle shear failure. From that perspective, the current gap is both theoretical: "How can shear distress be identified prior to the development of the critical shear crack in a brittle manner?" as well as practical "Which indicators and measurements can be developed for the practical application in proof load testing?". This paper addresses the need for defining a complete set of shear stop criteria, that are easy to measure, broadly applicable, and have a solid theoretical basis. To come up with stop criteria that can be used in practice, the shear stop criteria are used together with the flexural stop criteria and stop criteria for serviceability limit state in a traffic light system.

Description of Experiments

Slabs Strips

To develop and validate the proposed stop criteria, three series of experiments have been used. All experiments have been carried out in the Stevin II Laboratory of Delft University of Technology. The first series consists of slab strips (i.e. beams without shear reinforcements), the second series of straight reinforced concrete slabs, and the third series of skewed reinforced concrete slabs. The rationale for selection of these three series is as follows: the slab strips are used to develop shear stop criteria on non-shear-reinforced beam elements using current mechanical models. Then, the slab experiments are used to add slab behavior (transverse distribution). Finally, the skewed slab experiments are used to validate the proposed approach on the most complex type of slab bridge that can be encountered in practice.

The slabs strips are 10 m in length × 0.3 m in width, using heights of 500, 800, and 1200 mm.[26,27] The span length is 9 m. The strips are simply supported and subjected to a single concentrated load, see *Fig. 4*. The materials used for the experiments are concrete class C65/80 and ribbed reinforcement with $f_{ym} = 550$ MPa.

From this series of experiments, the so-called Delft shear tests carried out between 2016 and 2021[27], of 137 tested specimens, fourteen experiments were selected for the development and analysis of the stop criteria, see Table 1. The selection criteria included a distribution in varied parameters, as well as testing using various cycles, and measurements required for the stop criteria analysis. The table compiles information on the cube concrete compressive strength $f_{c,cube}$, the reinforcement ratio ρ_l, the shear span a, the effective depth to the longitudinal reinforcement d_l, the shear span to depth ratio $\lambda = a/d_l$, and the maximum load at shear failure P_u.

The relevant instrumentation consists of linear variable differential transformers (LVDTs) and the use of 2D DIC (Digital Image Correlation), see *Fig. 1c*. Postprocessing to obtain the displacement field is done with MatchID[28] software, and an in-house Matlab script[29] to find the average strain using virtual LVDTs. The crack pattern and kinematics are obtained using the automated detection and crack measurement (ACDM) software.[30]

Straight Slabs

A selection from a series of experiments on straight slabs is taken.[31] These slabs are 5 m × 2.5 m × 0.3 m. The experiments are selected based on the failure mode of shear, and with loading in the middle of the width to have slab behavior. It should be noted that this loading condition is not often used during proof load testing of slab members, where the loading is typically placed in the first lane. The slabs are supported on line supports composed of a steel beam (HEM 340) equipped with seven load cells to measure the reaction forces, see *Fig. 2a*. To create a continuous support, three Dywidag prestressing bars are anchored to the strong floor of the laboratory. A loading plate of 200 mm × 200 mm is used. The load is applied in cycles of loading and unloading, similar to the loading protocol used in a proof load test.

Four slabs reinforced with ribbed bars ($f_{ym} = 583$ MPa and $f_{um} = 706$ MPa) and two with plain bars ($f_{ym} = 304$ MPa and $f_{um} = 442$ MPa, tested on Ø25 mm bars) are cast. The slabs with ribbed bars (indicated with SR) have a reinforcement ratio of 0.99% and effective depth of 265 mm, and the slabs with plain bars (indicated with SP) have $\rho_l = 2.02\%$ and $d = 262.5$ mm, see *Fig. 2b and c*. Concrete class C35/45 is used for all specimens. For the study of the stop criteria, a subset of experiments is selected for which the load is placed in the middle of the width (indicated with "M" in the experimental code), and thus full slab behavior occurred in

Test name	$f_{c,cube}$ (MPa)	ρ_l (%)	a (mm)	d (mm)	$\lambda = a/d$	P_u (kN)
H602	86	0.57	4500	1158	3.89	306
H401	81	0.42	4500	1158	3.89	264
H403	82	0.42	4500	1158	3.89	350
H404	82	0.42	4000	1158	3.45	269
H121	84	1.14	3000	1145	2.62	341
B501A1	81	1.15	2500	455	5.5	277
B501B1	76	1.15	1500	455	3.3	210
B502B1	77	0.68	1750	455	3.8	155
E801A1[a]	84	0.64	2000	770	2.6	213
E801B1	91	0.64	2000	770	2.6	205
E802A1	76	0.83	2000	740	2.7	219
E802B1[a]	76	0.83	2000	740	2.7	270
E803A1	83	0.82	3500	760	4.6	279
E803B1	83	0.82	3500	760	4.6	308

[a]Specimens with $P_u = P_{cr}$ (load level at which the critical shear crack opened).

Table 1: Overview of analyzed slab strips

the experiment. Table 2 gives an overview of the five evaluated experiments for the stop criteria on straight slabs. 2D DIC, 3D DIC, LVDTs, lasers, and acoustic emission sensors are used as instrumentation to support the development of stop criteria.[33] *Fig. 2d-f* shows the details of lasers, LVDTs and DIC measurements.

Skewed Slabs

15 experiments are carried out on five skewed slab members with a span length of 3.6 m, width of 2 m and thickness of 300 mm,[35] see *Fig. 3a*. The concrete strength class is C35/45 and the reinforcement is B500B, with a longitudinal reinforcement ratio of 0.996%. The reinforcement is applied in an orthogonal layout (with longitudinal and transverse reinforcement crossing at 90°) and non-orthogonal layout (with the longitudinal and transverse reinforcement in parallel to the free edges of the specimen), as illustrated in *Fig. 3b and c* for the 60-degree crossing angle specimen.

The size of the loading plate is 200 mm × 200 mm, and the line supports are 100 mm wide. 2D DIC, 3D DIC, LVDTs and lasers are used as instrumentation[36], see *Fig. 3d-f*. For the analysis of the stop criteria, experiments with $a/d = 3$ are filtered because of the position of the LVDTs on the specimens, resulting in the nine experiments selected for the analysis. Table 3 gives the test results of the experiments used for the validation of the stop criteria selected from the series of skewed slab experiments, indicating the measured concrete compressive strength $f_{cm,cube}$ at the age of testing, the shear-span-to-depth ratio a/d and the maximum externally applied load in the experiments, P_{max}. All experiments resulted in shear failures. Only experiments near the obtuse corner are selected for validation, as this critical location is used during proof load testing. As can be seen in *Fig. 3*, the hooks to the reinforcement may act as local shear reinforcement for testing near the edge. For these cases, and for the analysis of stop criteria in general, the analysis focuses

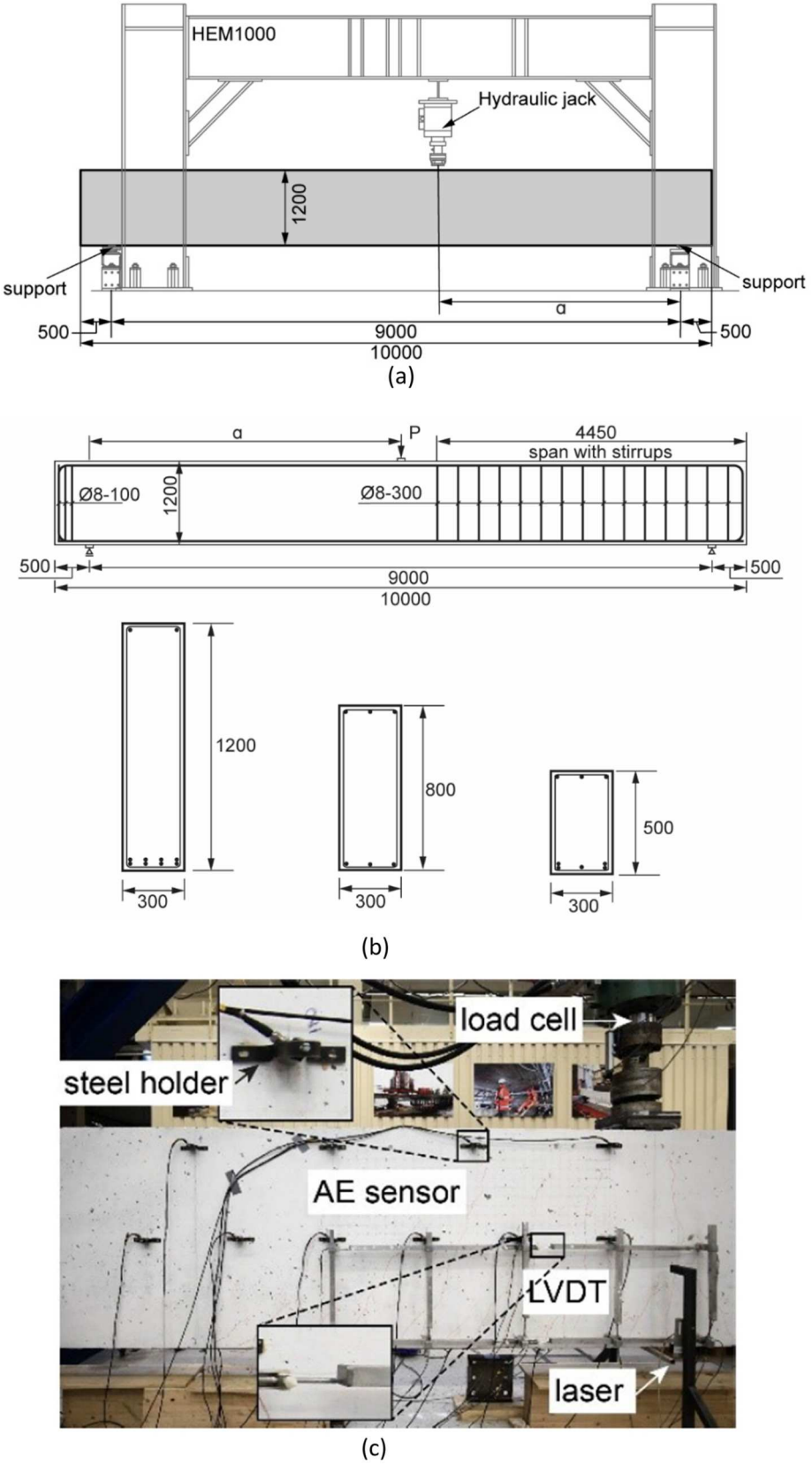

Fig. 1: Details of slab strip experiments: (a) Test setup used for slab strips[31]; (b) reinforcement layout of the slab strips. Units in [mm][27]; (c) instrumentation as illustrated on H601A[32]

on the development of the initial shear crack for the stop criterion and does not consider the influence of additional load-carrying mechanisms such as the contribution of the hooks near the edge, or the development of a direct compressive strut between the load and the support for cases with the load close to the support.

Shear Stop Criteria based on Mechanical Models

Beam Shear Stop Criterion based on the Critical Shear Displacement Theory

This section introduces the theory on which the shear stop criteria are based, as well as how shear theories can be rewritten in such a way that measurable parameters are clearly identified and can be compared to indicator values that are selected for the stop criteria. Aggregate interlock is one of the main shear-carrying mechanisms in members without shear reinforcement[37], together with dowel action, the contribution of the concrete in the compression zone to the shear capacity, and, to a lesser extent, tension across the crack (*Fig. 4*). In wide beams and slabs, aggregate interlock provides up to 70% of the shear capacity.[38,39] In addition, Ref. [40] showed that the contribution of aggregate interlock and dowel action is almost 90% for a beam with 1.97% of tension steel and $a/d = 2$, as compared to about 50% for a beam with 3.95% of tension steel and $a/d = 6$. For slab bridges, which typically have lower amounts of flexural steel, aggregate interlock is the dominant shear-carrying mechanism.

A stop criterion based on aggregate interlock should be linked to a measurable parameter. For the stop criterion, the simplified aggregate interlock expression of the Critical Shear Displacement Theory, CSDT,[42] is used. This theory uses the critical shear displacement Δ_{cr}, which is difficult to measure during a proof load test. Therefore, an expression based on the crack width w at the level of the tension steel and the acting shear stress τ at the cracked

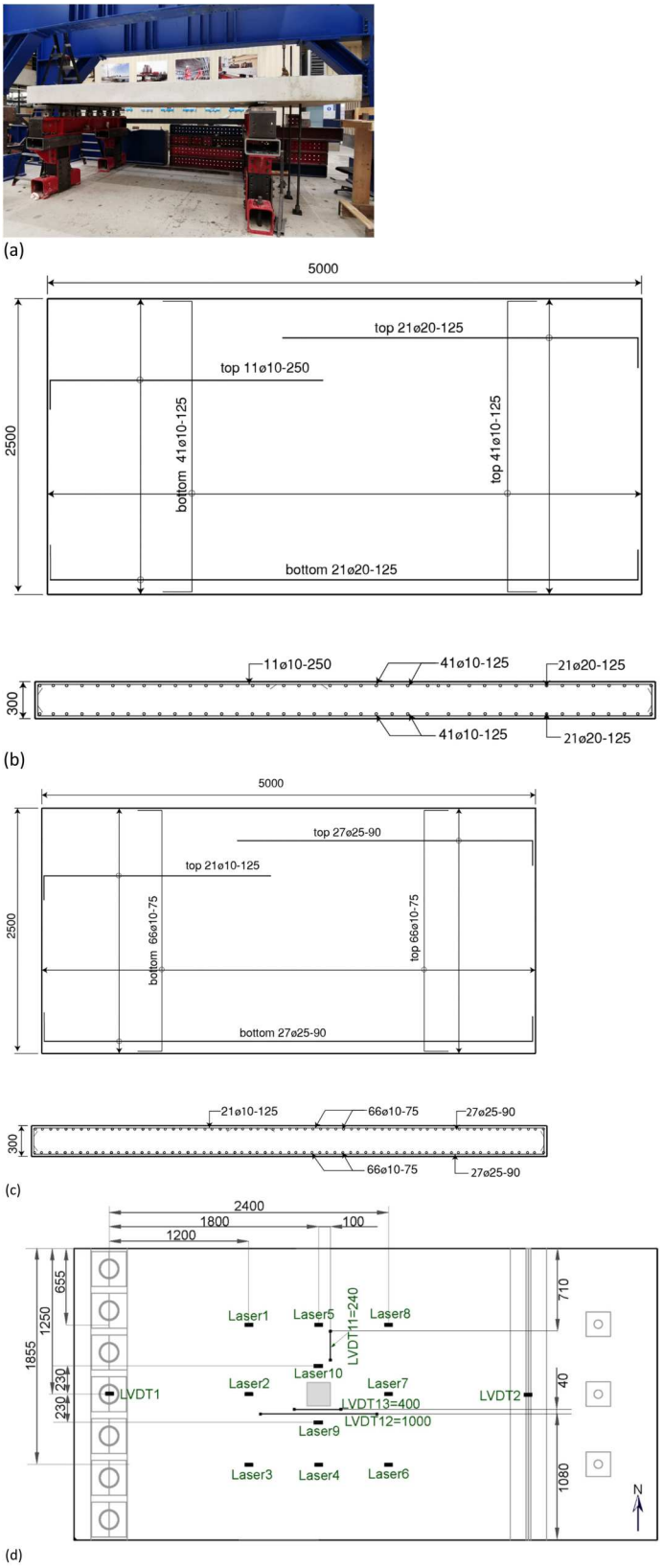

Fig. 2: Details of slab experiments. (a) Test setup photograph, (b) plan view and section of reinforcement layout for SR specimens, and (c) for SP specimens. All dimensions in mm[34]. Details of instrumentation: (d) top view showing lasers and LVDTs, (e) bottom view showing lasers and LVDTs from SR2M1, (f) DIC details applied to SR1M1[33]

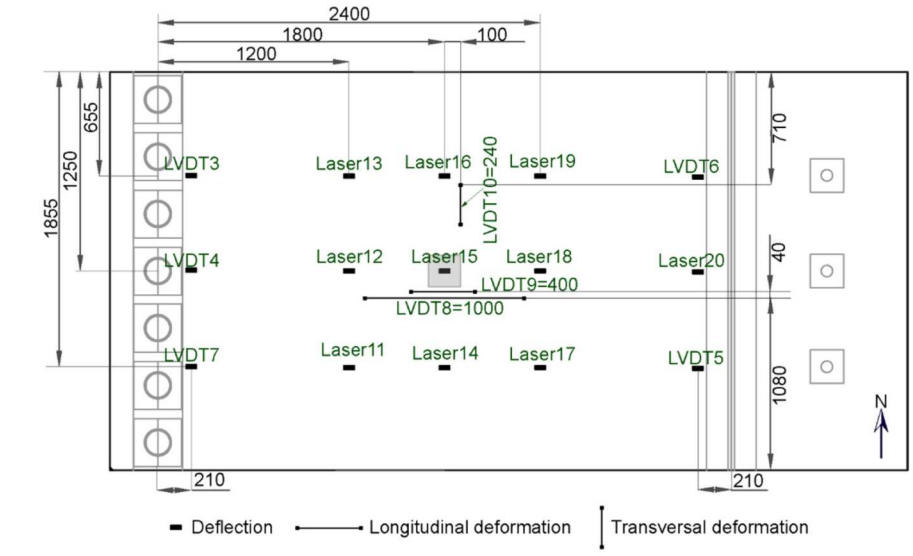

(e)

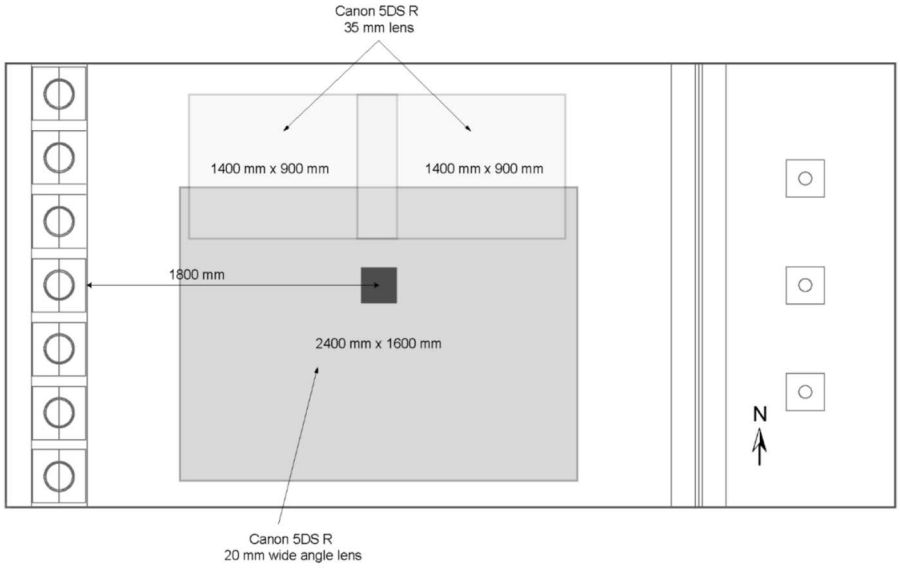

(f)

Fig. 2: Continued

section has been proposed.[43] Moreover, it is assumed that the aggregate interlock capacity V_{ai} can be taken as a lower bound for the shear capacity, given the large contribution of aggregate interlock to the shear capacity. In the CSDT, the aggregate interlock capacity is determined as:

$$V_{ai} = f_c^{0.56} s_{cr} b \frac{0.03}{w - 0.01} \\ (-978\Delta^2 + 85\Delta - 0.27) \quad (1)$$

In Eq. (1), f_c is the concrete compressive strength, s_{cr} is the height of a fully developed crack, b is the member width, w is the nominal crack width at the level of the steel reinforcement, and Δ is the shear displacement. Rearranging terms of Eq. (1) into Eq. (2) so that all measurable parameters are on the left-hand side of the equation and replacing the shear displacement Δ by the critical shear displacement Δ_{cr} results in:

$$V_{ai}(w - 0.01) = 0.03 f_c^{0.56} s_{cr} b \\ (-978\Delta_{cr}^2 + 85\Delta_{cr} - 0.27) \quad (2)$$

with the displacement at which the opened crack becomes unstable Δ_{cr} as given in Eq. (3):

$$\Delta_{cr} = \frac{25 d_l}{30610 \phi_{eq}} + 0.0022 \leq 0.025 \quad (3)$$

and the equivalent rebar diameter ϕ_{eq} as given in Eq. (4) *equation reference goes here*

$$\phi_{eq} = \frac{\Sigma \phi_i^2}{\Sigma \phi_i} \quad (4)$$

The height of the fully developed crack can be determined from flexural theory, hinging on the assumption that sectional analysis from flexural theory can be used for shear performance, as:

$$s_{cr} = \left(1 + \rho_l n - \sqrt{\rho_l n + (\rho_l n)^2}\right) d \quad (5)$$

with in Eq. (5) ρ is the reinforcement ratio, n is the ratio between the Young's modulus of the steel and the Young's modulus of the concrete, and d is the effective depth to the longitudinal reinforcement. The left-hand side of Eq. (2) can be simplified into the shear indicator I_{CSDT}, and the indicator relating the shear stress τ (derived from the sectional shear V, which will be considered equal to V_{ai} at failure) and nominal

Test no.	Age [days]	$f_{c,cube}$ [MPa]	SS/CS	a [mm]	d [mm]	a/d	ρ_l	P_{max} [kN]	V_{max} [kN]
SR2M3[a]	204	60.19	SS	800	265	3.02	0.99%	1187	911
SR3M1	103	65.65	SS	800	265	3.02	0.99%	1141	862
SR3M2	110	65.58	CS	1200	265	4.53	0.99%	1149	858
SP1M3	75	62.08	SS	800	262.5	3.05	2.02%	1135	886
SP2M1	99	62.59	SS	800	262.5	3.05	2.02%	1291	1007

[a]A secondary punching failure mode was observed.

Table 2: Summary of tests on straight slabs: all tests resulted in a shear failure after loading in the middle of the width

Test	Age [days]	$f_{cm,cube}$ [MPa]	a/d	P_{max} [kN]
S60N2Ac1	102	64.7	3	615.3
S60N2Ac2	112	64.7	3	573.8
S60O1Auc	123	69.4	3	580.1
S60O1Ac	131	69.4	3	544.5
S60N1Auc	152	65.1	3	606.4
S45N1Auc	259	72.3	3	420.8
S45N1Ac	274	72.3	3	508.4
S75N1Auc	302	70.47	3	745.9
S75N1Ac	308	70.47	3	599.7

Table 3: Skewed slabs test results for analyzed experiments

crack width w becomes as follows:

$$I_{CSDT} = \frac{V(w-0.01)}{bs_{cr}} \approx \frac{V(w-0.01)}{bd_l} = \tau(w-0.01)$$

The critical shear indicator $I_{CSDT,cr}$ (given in Eq. (7)) then becomes a single value as stop criterion that can be used to compare against during the experiment using measured sectional shear and crack width per Eq. (6):

$$I_{CSDT,cr} = 0.03 f_c^{0.56} \frac{s_{cr}}{d_l} (-978\Delta_{cr}^2 + 85\Delta_{cr} - 0.27) \quad (7)$$

with Δ_{cr} from Eq. (6) and s_{cr} from Eq. (5).

Beam Shear Stop Criterion based on the Critical Shear Crack Theory

In the Critical Shear Crack Theory, CSCT[44], the shear strength depends on the crack width and roughness of a critical shear crack (expressed as a function of the maximum aggregate size d_g). One of the main assumptions in the theory is that the critical crack width w can be taken as proportional to the multiplication of longitudinal strain ε_x and d_l at a control depth of $0.6d_l$ from the top fiber. As such, one of the main assumptions of the CSCT is the link between flexural performance and sectional analysis, and shear performance. The shear resistance V_R is expressed as:

$$\frac{V_R}{bd_l\sqrt{f_c}} = \frac{1}{6}\frac{2}{1+120\frac{\varepsilon_x d_l}{16+d_g}} \quad (8)$$

with in Eq. (8) f_c is the concrete compressive strength (in MPa), b is the width, d_l is the effective depth, ε_x is the longitudinal strain at the control depth derived from the bending moment demand in the critical section, and d_g is the maximum aggregate size (in mm). Replacing the shear resistance V_R with the sectional shear V, an indicator can be derived with f_c in MPa and d_g in mm:

$$\frac{V}{bd_l\sqrt{f_c}} = \frac{1}{6}\frac{2}{1+120\frac{\varepsilon_x d_l}{16+d_g}}$$
$$I_{CSCT} = \frac{V}{bd}\left(1+120\frac{w}{d_g}\right) = \tau\left(1+120\frac{w}{d_g}\right) \le \frac{\sqrt{f_c}}{3} \quad (9)$$

In Eq. (9), the measurable parameters are V (as a function of the applied load) and ε_x, which can be derived from the strain at the level of the tension reinforcement and assuming a linear strain distribution as:

$$\varepsilon_x = \frac{0.6d_l - c}{d_l - c}\varepsilon_{x,rebar} \quad (10)$$

with in Eq. (10) d *represents* the effective depth and c represents the height of the compression zone.

Influence of Precracking

Previous research regarding stop criteria on beams indicated a difference in behavior for members previously cracked in bending as compared to members uncracked in bending.[45] The experiments on slabs subjected to a proof load testing protocol showed that the overall shear behavior in terms of strain development of precracked slabs and those not previously tested was similar. The maximum load was lower for precracked slabs than for slabs not previously tested: the average capacity of a slab with predamage is 88.7% of the capacity of a slab without predamage, with a coefficient of variation of 13.9%. The flexural behavior is different: the precracked specimens demonstrate a lower stiffness due to the cracking exerted in the previous loading stages and it is possible that some permanent deflection is present. The effect of pre-existing cracking on the average concrete tensile strains can be accounted for in the strain-based shear stop criterion with a factor of 0.78.[46]

Critical Location for Beam Members

When these stop criteria need to be applied to slab strips or beams, the location of the measureable parameters needs to be identified as well. Therefore, this section makes a step from the theoretically derived stop criteria to the practical advice on where to measure and how to interpret the results. As shown in *Fig. 5*, three different critical regions emerge for the behavior in reinforced concrete beam members without shear reinforcement:

- a flexural region of $0.5d$ from the concentrated load, for cracking stop criteria related to the Serviceability Limit State (green region in *Fig. 5*),
- a region with large M/Vd, identified as $0.8 < M/Vd \times (1/\lambda) < 1$ with $\lambda = a/d$ to account for shear slenderness in which the shear stop criteria are reached first (yellow region in *Fig. 5*),
- a region with low M/Vd, identified as $M/Vd \times (1/\lambda) < 0.7$ in which the shear stop criteria are reached later (red region in *Fig. 5*).

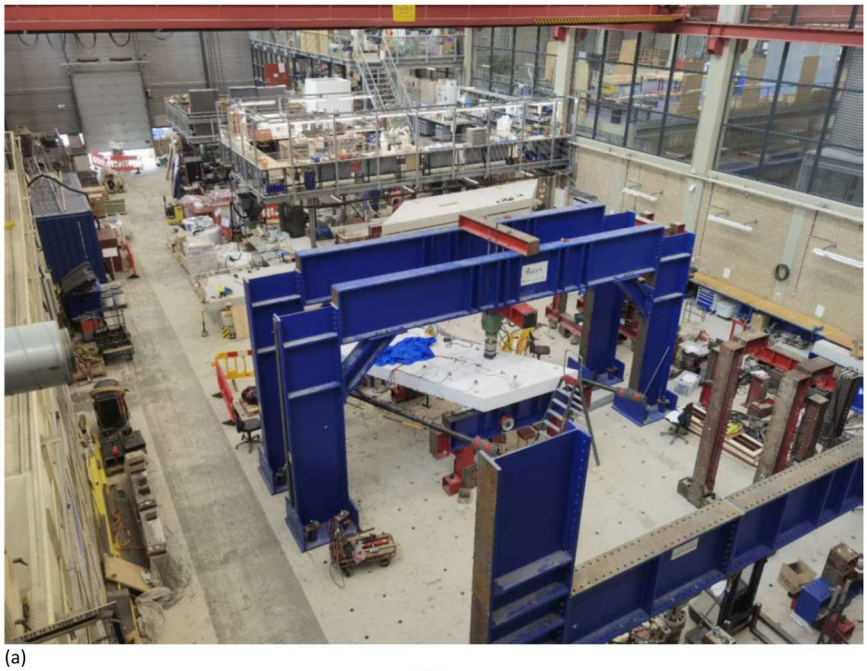

(a)

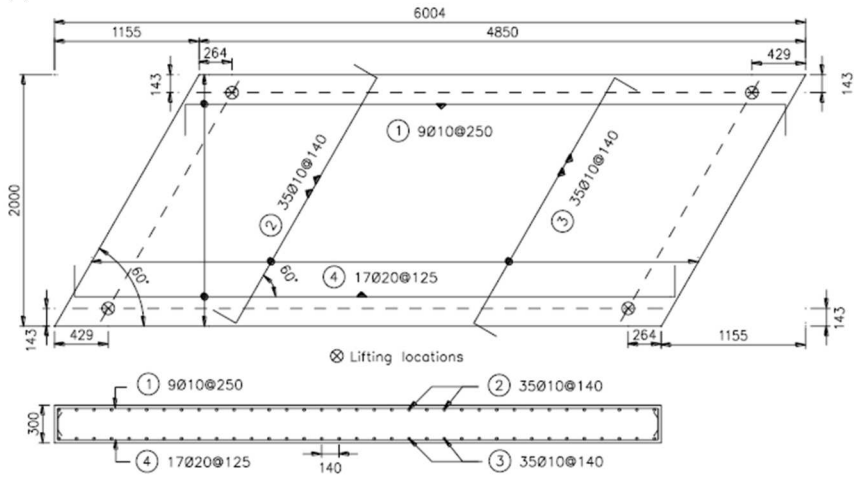

(b)

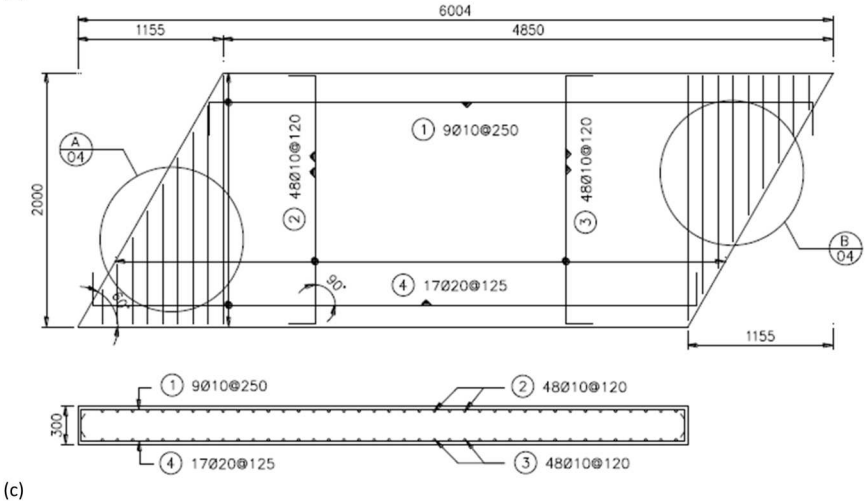

(c)

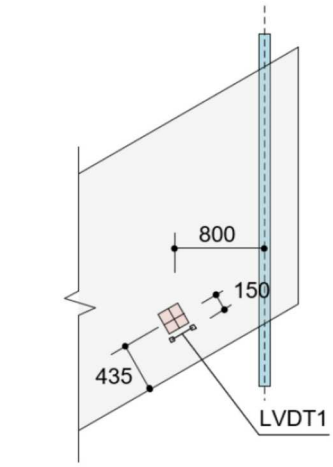

(d)

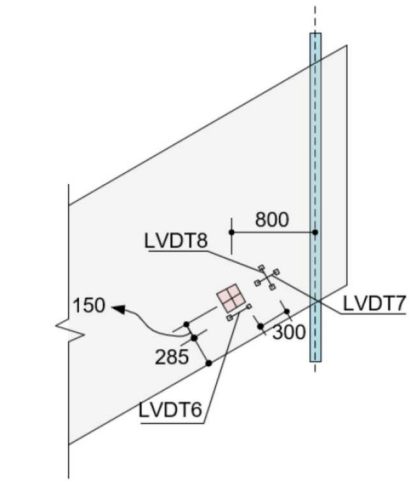

(e)

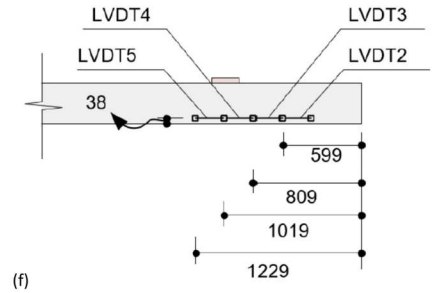

(f)

Fig. 3: Details of skewed slab experiments: (a) photograph of test setup: (b) Reinforcement layout of skewed slabs illustrating specimens S60N1 and S60N2; (c) Detailed drawing of specimen S60O1; layout of the LDVTs: (d) top view; (e) bottom view; (f) side view[36]. All dimensions in mm

Fig. 3. Continued

Application to Slab Members

Missing Link for Slab Members

To extend the stop criteria developed for beam members without shear reinforcement[47] to reinforced concrete slabs without shear reinforcement subjected to concentrated live loads, adjustments are necessary. The considerations that are necessary for

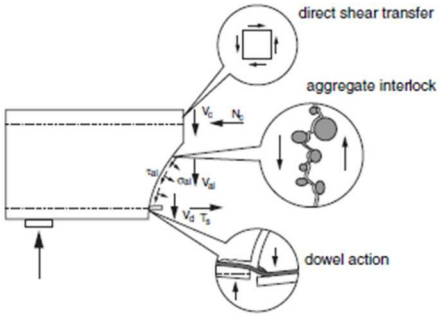

Fig. 4: Shear-carrying mechanisms, reprinted from Ref. [41] with permission

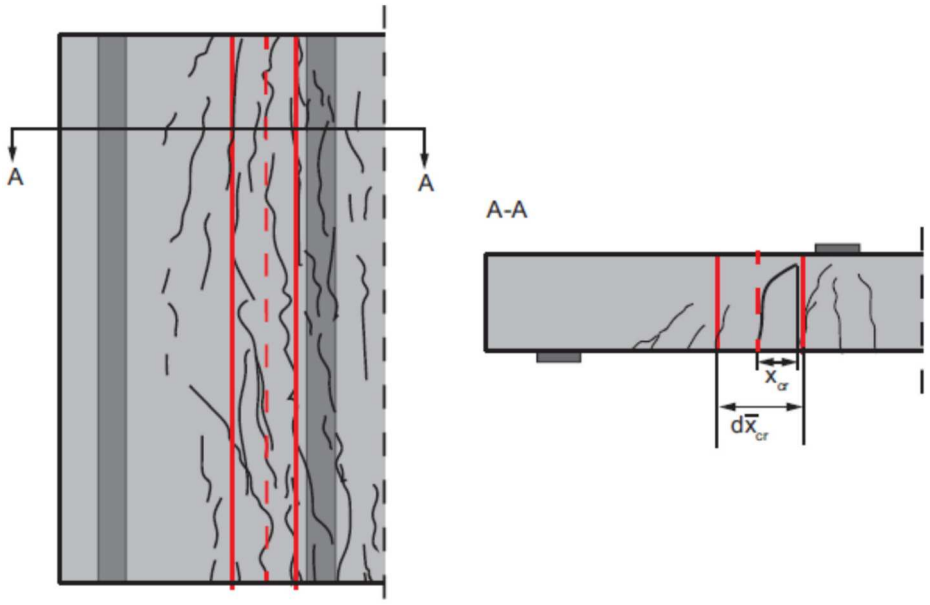

Fig. 6: Sketch of crack pattern of a reinforced concrete slab subjected to a line load (showing bottom face and section A-A), evidencing the waviness of the transverse crack profile. Modified from Ref. [48]

these adjustments are both theoretical (how to consider transverse distribution) as well as practical (where to measure). From that perspective, this section will both rely on shear theory as well as analysis of tested experiments to come to practical recommendations. The transverse distribution of forces needs to be considered, as well as the non-constant bending moment and shear force distribution along the width of the slab. Moreover, in wide members the crack profile is wavy in the transverse direction,[48] see *Fig. 6*. This irregularity increases the cracking surface and improves aggregate interlock, resulting in an increased one-way shear capacity. To account for this, a slab factor and effective width are proposed.

In terms of measurable responses, for slabs under concentrated loads the shear crack forms gradually: first the shear crack opens at the locations close to the concentrated load, and then it continues to open in the transverse direction. As such, it is recommended to monitor strains and crack development in the width direction, and the assumption is that the shear indicators will be reached first in the region close to the concentrated load and later at sections farther away in the transverse direction.

Critical Location for Slab Members

The *M/Vd* ratio is a proxy to describe the relationship between the bending moment, the sectional shear, and the crack profile in beams, as resulting from the externally applied loads. As shown in *Fig. 6*, the crack profile is nearly straight at high *M/Vd* ratios (close to the load), whereas for low *M/Vd* (near the support) the cracks are more inclined and open at higher load levels.

Slab moments can be represented by M_x, M_y or the torsional moment M_{xy}, as well as the principal bending moment M_1 and M_2. In the subsequent analyses, the principal bending moment M_1 is used to represent the principal sagging moment and to derive the *M/Vd* ratio in slabs, which is linked to the crack width, and thus aggregate interlock and shear capacity. The principal moment can be derived as given in Eq. (11):

$$M_1 = \frac{M_x + M_y}{2} + \sqrt{(M_y - M_x)^2 + 4M_{xy}^2} \quad (11)$$

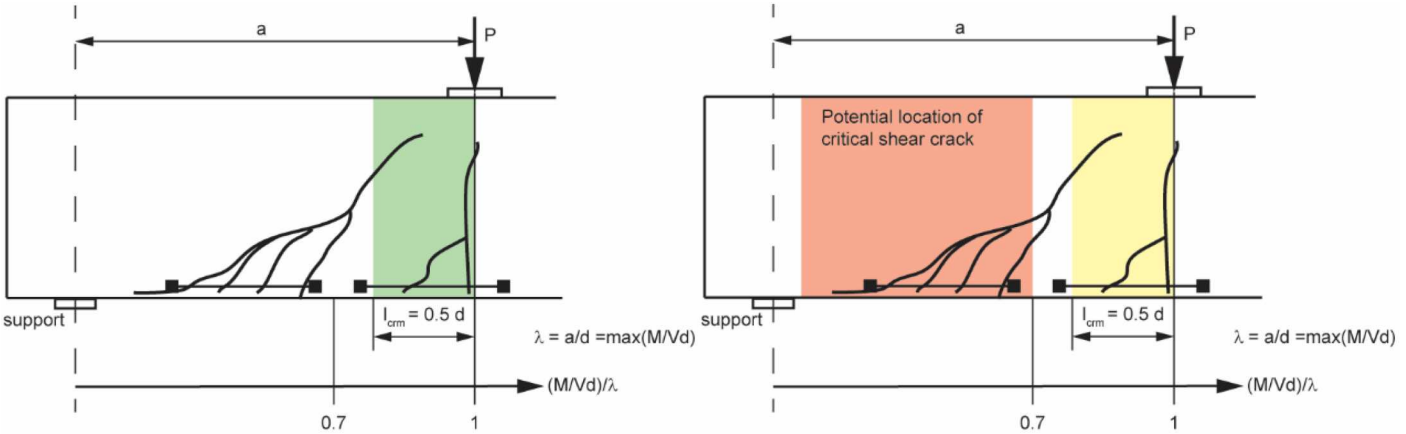

Fig. 5: Overview of stop light system and critical regions for shear stop criteria for RC slab strips, from Ref. [47] (permitted reuse of open access contents)

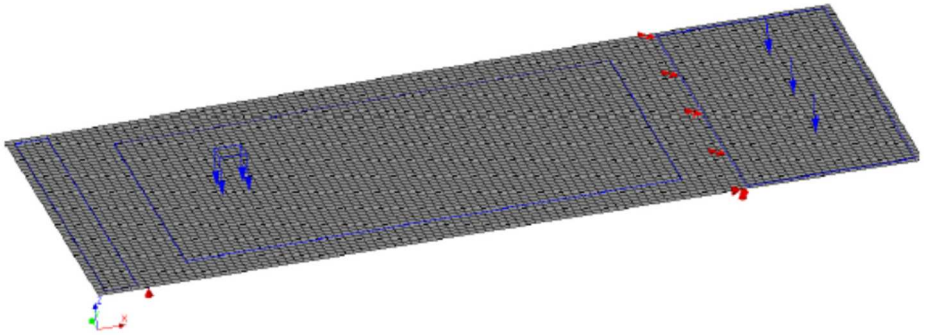

Fig. 7: Linear finite element model of SR3M1 showing mesh, loads and boundary conditions

The associated principal direction is given in Eq. (12):

$$\alpha_1 = \frac{M_x - M_1}{M_{xy}} \tag{12}$$

The shear field can be defined as a vector field that describes the direction φ_o (see Eq. (13)) and the magnitude v_0 of the principal shear force per unit length of a loaded slab (see Eq. (14)).[49] The magnitude and direction of the principal shear force is derived from the unitary shear forces v_x and v_y:

$$\phi_o = \arctan\left(\frac{v_y}{v_x}\right) \tag{13}$$

$$v_0 = \sqrt{v_x^2 + v_y^2} \tag{14}$$

To find the critical location in slab members, the bending moment and shear force fields are determined using a linear finite element model in DIANA. The slabs are modeled using 8-node quadrilateral shell elements with an average element dimension of 50 mm, see *Fig. 7*. To account for cracking and load redistribution[50], the Poisson ratio is taken as $\upsilon = 0$ and the shear modulus is taken as $G = E/16$. The resulting principal moment distribution and shear field, as well as post-processed *M/Vd* distribution is shown in *Fig. 8*.

The shear flow vector distribution in *Fig. 8*, indicates that close to the loading point, shear is carried in both directions, and that the shear flow becomes uniform and representative of one-way shear close to the support. Moreover, the shear flow shows that shear is not carried by the full slab width but remains concentrated in the central region. The distribution of *M/Vd* in *Fig. 8* shows the regions with high *M/Vd* and the regions with low values of *M/Vd*. The regions with low values of *M/Vd* are close to the loading point, where highly inclined cracks can develop. The region with $M/Vd \approx 2.5$ aligns with the location of the shear crack as observed in the experiments and shows a fan-like shape.

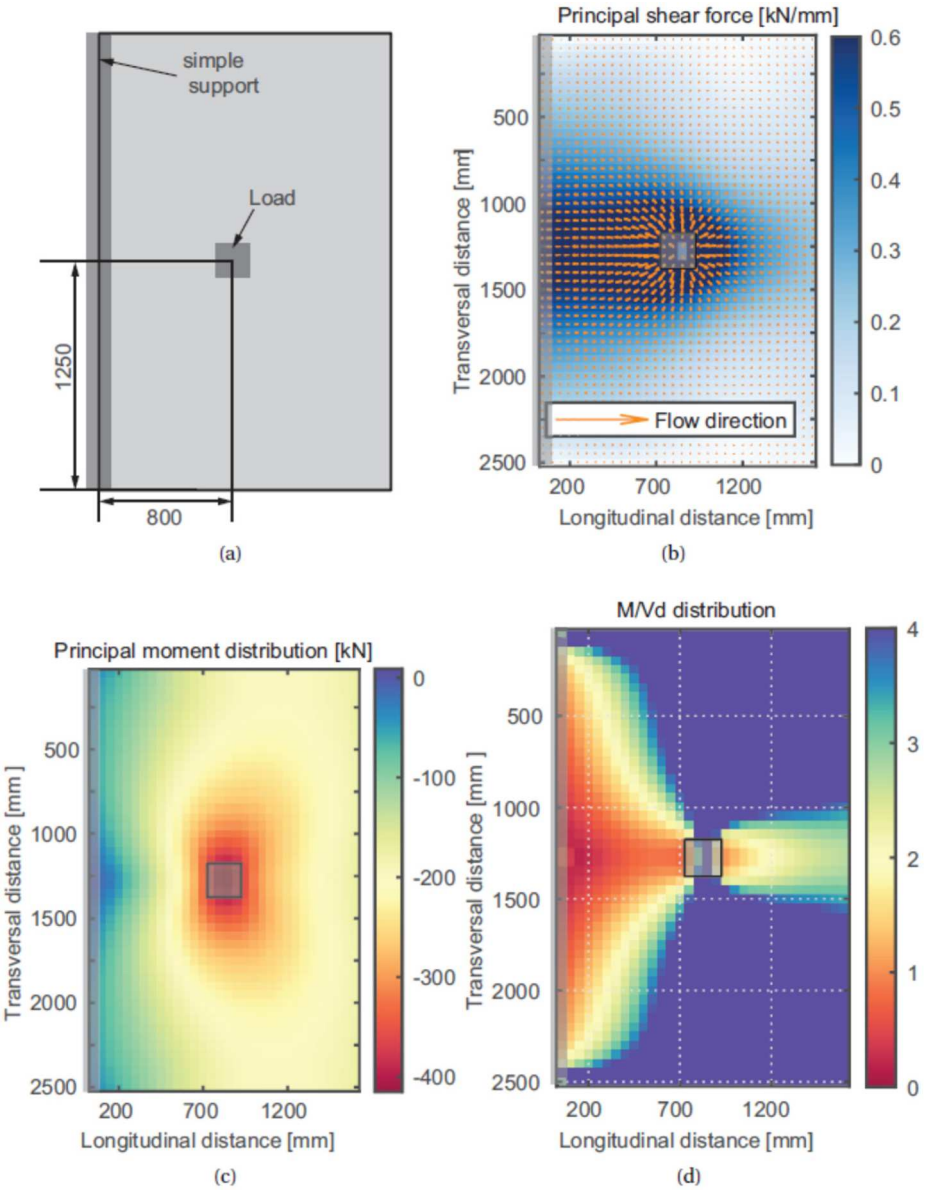

Fig. 8: Shear field and M/Vd *distribution for test SR3M1 (a) Sketch of SR3M1, (b) Principal moment distribution, (c) Shear field distribution, and (d)* M/Vd *distribution*[51]

Considerations for Waviness of Crack Profile

The way in which the waviness of the crack shape influences the contribution of aggregate interlock considered in the Critical Shear Displacement Theory is identified as follows:[48]

- The wavy crack profile results in an overall increased length of the crack profile. As a result, the shear force transferred through aggregate interlock can be increased by:

$$V_{ai}^{'} = \frac{b_{cr}}{b} V_{ai} \tag{15}$$

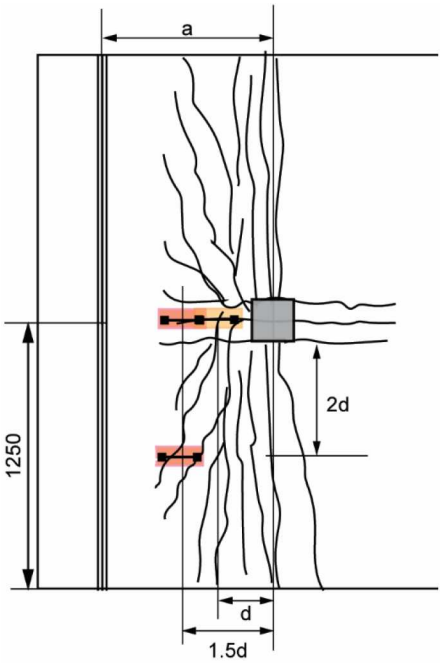

Fig. 9: Overview of the monitored positions for the yellow and red light stop criterion

where in Eq. (15) b_{cr} is the real length of the critical crack in the transverse direction.

- A shift in the position of the crack in the longitudinal direction occurs, see *Fig. 6*. Considering this shift, an increase of the critical shear displacement is necessary as a result of the crack profile:

$$\Delta' = \theta(x_{cr} + d\widetilde{x}_{cr}) = \Delta_{cr}\left(1 + \frac{d\widetilde{x}_{cr}}{x_{cr}}\right) \quad (16)$$

where in Eq. (16) x_{cr} is the length of the critical crack from the tip to the root in the longitudinal direction, and $d\widetilde{x}_{cr}$ is the average variation of the transverse crack profile in the longitudinal direction. To simplify the description of the crack profile, a random triangular wave profile is assumed. The amplitude A_p of the transverse crack is related to its variation in the longitudinal direction, and therefore related to the maximum crack spacing defined by the bond between the reinforcement and the concrete. The average amplitude is equal to the average crack spacing $l_{cr} = \Psi_s l_t$ with $\Psi_s = 1.5$and

$$l_t = \frac{f_{ctm}\phi}{4\tau_{bm}\rho_{eff}} \quad (17)$$

where in Eq. (17) l_t is the transfer length, τ_{bm} is the average bond between reinforcement and concrete, $\rho_{eff} = \frac{A_s}{A_{c,eff}}$is the effective reinforcement ratio, φ is the reinforcement diameter, and f_{ctm} is the mean tensile strength of the concrete.

The wave length of the crack profile is related to the length of the influencing zone of a local crack in the transverse direction. The position of a new crack will not be influenced by the adjacent crack, which could generate a next peak in the wave profile. The distance between two peaks is half the average wave length. This problem was approached by Ref. [48] by considering a local force in a beam on elastic foundation. The final expression of the influencing length l_w in a slab is determined as:

$$l_w = \pi\sqrt[4]{\frac{4EI_x}{k_w}} = \pi\sqrt[4]{\frac{4x^2(l-x)^2 d_x}{3l}} \quad (18)$$

with in Eq. (18) l represents the length of the slab, x denotes the distance of a local weak spot to the support, d_x the width of the transverse strip of the slab, which can be approximated to the average crack spacing l_{cr}.

This estimation of the amplitude and wave length serves to evaluate the real crack length and critical shear

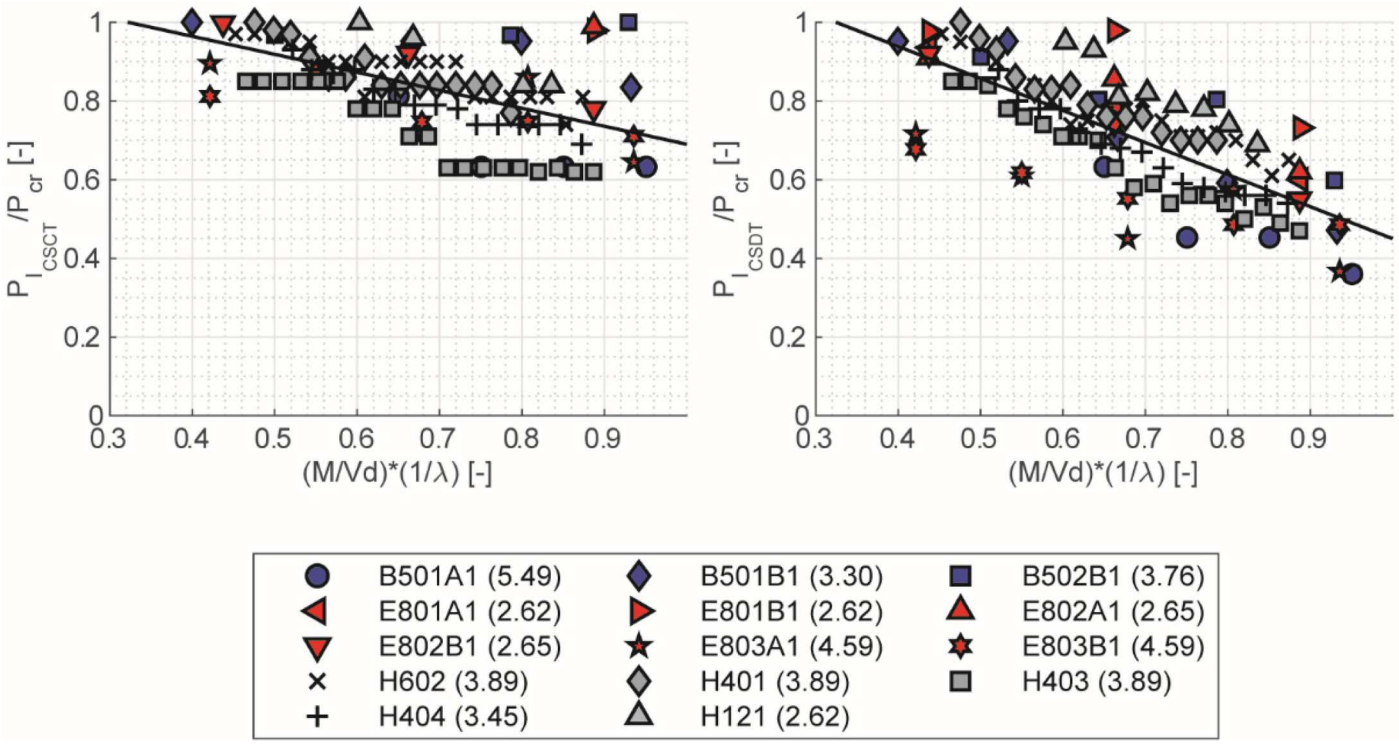

Fig. 10: Results of the indicator based on the Critical Shear Crack theory and the Critical Shear Displacement Theory as a function of M/Vd normalized by factor λ[47]

displacement. For this approach, $d\tilde{x}_{cr}$ in Eq. (19) can be estimated as $d\tilde{x}_{cr} = \frac{A_p}{2}$ resulting in the increment of the critical shear displacement as given in Eq. (19)

$$b_{cr} = b\frac{T}{\sqrt{T^2 + A_p^2}} \tag{19}$$

From the analysis of experiments on slabs subjected to line loads, the average increase is 18.2% and the method was found to be able to relate the width to the shear capacity.

As a result of these considerations, for the slabs, the value of Δ_{cr} was multiplied by a factor of 1.27, to account for the wavy crack profile and the additional displacement needed for the slab behaviour. The locations of particular interest to apply the shear stop criteria are identified in Table 9 for the yellow and red light shear stop criteria. The critical locations for the measurement are adapted to slabs as shown in *Fig. 9*.

Validation of Stop Criteria with Experiments

The proposed shear stop criteria are validated with the three sets of experiments. For efficiency, not all parameters are varied in all series of experiments. For example, the effect of the longitudinal reinforcement ratio is addressed in the slab strip experiments, whereas the added complexity of the width is addressed by the slab experiments and the additional complexity of skewness by the skewed slab experiments. In the skewed slab experiments, the instrumentation was applied to capture beam shear behavior. For the skewed slab test, the LVDT sensor layout was prepared based on M/Vd rather than $M/Vd \times 1/\lambda$[52]. As a result, the LVDTs used in the skewed slab experiments do not cover the yellow zone. An example of the results for the slab strips is displayed in *Fig. 10*.

Series of experiments	AVG [%]	STD [-]	COV [%]	% chance of > 100%
Slab strips	55	0.10	18%	3.4×10^{-4}%
Slabs	48	0.07	14%	5.5×10^{-12}%
Skewed slabs	67	0.19	29%	4.12%

Table 4: Validation of yellow light stop criterion I_{CSDT}

Series of experiments	AVG [%]	STD [-]	COV [%]	% chance of > 100%
Slab strips	77	0.13	16%	3.84%
Slabs	43	0.09	21%	1.2×10^{-8}%
Skewed slabs	76	0.13	18%	9.12%

Table 5: Validation of yellow light stop criterion I_{CSCT}

For all experiments considered, the stop criteria indicators are calculated, the load at which the stop criterion is reached P_{stop} is registered, and this load is divided by the maximum load in the experiment P_u to find the percentage of the maximum load at which a stop criterion is reached. For the slab strips, beam stop criteria are used. For the slabs, slab stop criteria are used, and for the skewed slabs, beam stop criteria are used because the load was applied near the edge and mostly one-way shear behaviour is observed. The results for I_{CSDT}, the results for the yellow light are given in Table 4 and for the red light in Table 7, and for I_{CSCT} the validation of the yellow light stop criterion is given in Table 5 and of the red light stop criterion in Table 7. The individual results and calculations can be consulted in the detailed background report.[53]

The results in Table 4 show that the performance of the yellow light stop criterion and the uncertainties are comparable throughout the three series. For the skewed slabs, the results have higher uncertainties, which can be partially explained by the fact that the measurements are taken outside of the recommended range for $M/Vd \times (1/\lambda)$ for the yellow light stop criterion. The average value of P_{stop}/P_u is in line with the expected value for a yellow light stop criterion (around 50% of the failure load) and the coefficient of variation is low, indicating adequate performance. Table 5 provides the validation on the yellow light stop criterion I_{CSCT}. The overall results are quite similar to the findings for the yellow light stop criterion I_{CSDT}. For certain cases I_{CSDT} performs better, whereas for other cases I_{CSCT} gives better results. As such, it is recommended to use both stop criteria for the yellow light criterion, as these are based on different mechanical models, and thus unearth different aspects of the shear behavior.

For the red light stop criterion, Table 6 contains the results for I_{CSDT}. It can be seen that the stop criterion has a lower percentage at which the stop criterion is reached for slabs than in beams. This observation can be explained by the redistribution capacity in slab members, which does not occur in beam members. The coefficient of variation is generally similar for the three studied sets of experiments. The average value is in line with the expectation of a red light stop criterion, allowing for an additional margin of safety during the execution of a proof load test. Considering the nature of the problem (indicators of shear prior to failure), the values of the coefficient of variation are good as they are less than 20%. Table 7 shows the performance of the red light stop criterion I_{CSCT}. This stop criterion works well for the beams and the skewed slabs, and appears to be more conservative for the slab members. This observation underlines the need to combine two indicators for stop criteria that are based on different mechanical models, so that they can capture different shear effects.

In addition, to quantify the percentage of cases for which the shear stop criterion is not achieved at failure, the distribution function assuming a normal distribution is developed, using the average and standard deviation values reported in Table 4 through Table 7. From the cumulative distribution function, the percentage of values for which $P_{stop}/P_u \geq 1$ is determined, see *Fig. 11*. The determined values are added to the final column in Table 4 through Table 7.

The results of the statistical analysis show that the highest probability of a

Series of experiments	AVG [%]	STD [-]	COV [%]	% chance of > 100%
Slab strips	80	0.12	13%	4.78%
Slabs	67	0.09	13%	0.01%
Skewed slabs	61	0.11	18%	0.02%

Table 6: Validation of red light stop criterion I_{CSDT}

Series of experiments	AVG [%]	STD [-]	COV [%]	% chance of > 100%
Slab strips	88	0.08	12%	6.68%
Slabs	44	0.06	15%	0%
Skewed slabs	76	0.10	14%	0.82%

Table 7: Validation of red light stop criterion I_{CSCT}

shear stop criterion not warning before failure lies with the yellow light stop criterion I_{CSCT} for the skewed slabs. However, the location of the LVDTs for these experiments was not ideal. Moreover, the reader should note that this result does not mean that 9% of all proof load tests will result in a failure of the bridge before the I_{CSCT} is achieved. The probability of failure during the proof load test is a conditional probability of the applied load. Research on the use of measurement data during proof load testing also provides a methodology on how to determine the probability of failure during and after a proof load test.[54]

Development of Comprehensive Traffic Light System

Flexural Stop Criteria at Yellow and Red Light

To take the previously described theoretically derived shear stop criteria and implement these into a guideline for proof load testing would not be sufficient. In addition, other indicators such as those developed using different structural responses can be added as these are complimentary, and other failure mechanisms, in particular flexure, should be included in the recommendation. This section brings together the previously discussed shear stop criteria, other indicators developed previously, and adds the flexural stop criteria.

Previous research developed a set of stop criteria for flexure.[55] Theoretically derived quantitative stop criteria were used as well as qualitative stop criteria. To align the flexural stop criteria with the traffic light system developed for shear, yellow and red light stop criteria for flexure are needed. For the yellow light stop criteria, part of the original flexural stop criteria are kept. These are: residual crack width, stiffness reduction of maximum 25%, changes to the horizontal or vertical deformation profiles, and changes to the load-displacement diagram. The residual crack width limit used is $w_{res} \leq 0.2w_{max}$ for members previously cracked in bending and $w_{res} \leq 0.3w_{max}$ for members not previously cracked in bending.

The new red light stop criterion is based on the previously determined flexural stop criteria. Two indicators are used: a strain limit and a crack width limit. The red light stop criterion strain limit ε_{stop}:

$$\varepsilon_c \leq \varepsilon_{c,bot,\max} - \varepsilon_{c0} = \varepsilon_{stop} \qquad (20)$$

with the bottom strain from Eq. (20) determined from sectional analysis in Eq. (21) as:

$$\varepsilon_{c,bot,max} = \frac{h-c}{d-c} \times \frac{f_{ym}}{E_s} \qquad (21)$$

where

ε_{c0} analytically determined short-term strain in the concrete caused by the permanent loads

$\varepsilon_{c,bot,max}$ concrete strain at the bottom of cross-section that corresponds to yielding of the steel

f_{ym} is the average yield strength of the tension reinforcement steel

E_s modulus of elasticity of reinforcing bars

The red light stop criterion for crack width w_{stop} is determined as given in

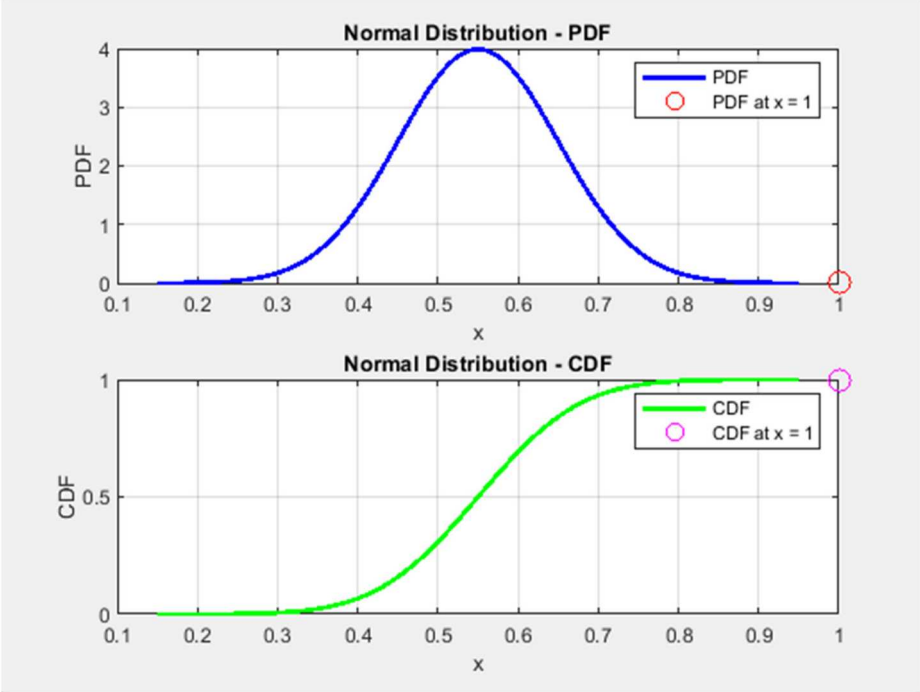

Fig. 11: Probability density function and cumulative distribution function for the normal distribution with AVG = 55% and STD = 0.10

	AVG	STD	COV
Yellow light flexure	56%	0.15	26%
Red light flexure	75%	0.11	15%

Table 8: Statistical results of the traffic light system of flexural stop criteria

Eq. (22):

$$w_{stop} = 2\frac{f_{ym} - f_{perm}}{E_s}\beta_{fr}\sqrt{d_c^2 + \left(\frac{s}{2}\right)^2} \quad (22)$$

where

f_{perm} stress in the steel caused by the permanent loads

β_{fr} strain gradient factor used in the method of Frosch[56]

dc cover to the centroid of the tension reinforcement

s reinforcement spacing

The flexural stop criteria have been checked on the beam experiments carried out earlier[45] provide the statistical results of the validation of the flexural stop criteria against the Ruytenschildt bridge slab strips (RSB01F, RSB02A, RB02B, RSB03F) and slab strips cast in the laboratory (P804A1, P502A2). While the coefficient of variation on the yellow light stop criterion is significantly larger than the coefficient of variation on the red light stop criterion, it should be noted that the yellow light stop criterion is based on a different set of parameters, as it determines the first load at which one of the stop criteria of residual crack width, stiffness reduction, horizontal deformation profiles, or vertical deformation profiles is reached. As such, it is valuable to maintain the yellow light stop criterion to gain information about the global performance of the bridge structure. For the stop and acceptance criteria from ACI 437.2M-13[25] and the German guidelines,[57] the range of values at which the recommended set of stop or acceptance criteria was reached was large. Using the Ruytenschildt beams[58] for example, the range of P_{stop}/P_u for ACI 437.2M-13 was 0.18–0.55, with a number of stop criteria not achieved during the load test,

Objective	Indicator	Physical meaning	Action
Serviceability limit state	w_{avg}	Onset of cracking in reference region	Understand that section changes from uncracked to cracked
Serviceability limit state	AE-based green-light criterion	Wave-based signal of cracking detected	Understand that section changes from uncracked to cracked
Shear	$\min(I_{CSDT}, I_{CSCT})$ in $0.8 < M/Vd \times (1/\lambda) < 1$	Local reaching of lower bound of shear capacity from mechanical models	Intermediate warning level
Shear	$\min(I_{CSDT}, I_{CSCT})$ near load for loads in middle of width and in $0.8 < M/Vd \times (1/\lambda) < 1$ for loading near edge	Local reaching of lower bound of shear capacity from mechanical models	Intermediate warning level
Shear	Initiation of inclined cracks	Development of shear cracking	Intermediate warning level
Shear	AE-based yellow-light criterion	Cracking in the strut	Intermediate warning level
Shear	Damage ratio of 0.5	Half of the strut width deteriorated	Intermediate warning level
Shear	$\min(I_{CSDT}, I_{CSCT})$ in $< M/Vd \times (1/\lambda) < 0.7$	Shear-carrying mechanisms nearly achieved in critical region	Further loading can result in (local) collapse
Shear	$\min(I_{CSDT}, I_{CSCT})$ at $1.5d$ in the middle as well as at $2d$ in width direction from load for loads in middle of width and in $M/Vd \times (1/\lambda) < 0.7$ for loading near edge	Local reaching of aggregate interlock capacity	Further loading can result in (local) collapse
Shear	Further development of inclined cracks, typically monitored using DIC	Full shear cracking	Further loading can result in (local) collapse
Shear	Red-light AE criterion	Cracking in strut significantly reduces capacity	Further loading can result in (local) collapse
Shear	Damage ratio near 1	Almost entire strut width deteriorated	Further loading can result in (local) collapse
Flexure	Minimum of stop criteria for residual crack width, stiffness reduction, deflection profiles	Changes in flexural behavior and load distribution occurring	Intermediate warning level
Flexure	Minimum of stop criterion for limiting strain or limiting crack width based on yielding of steel	Local yielding of reinforcement steel	Further loading can result in (local) collapse

Table 9 Overview of proposed stop criteria, indicating the traffic light system color

and for the German guideline the range of P_{stop}/P_u was 0.18–0.98 (Table 8).

Green Light for Serviceability

The stop criterion for crack width for serviceability is expressed as given in Eq. (23) and is based on typical crack width limits

$$w_{avg} = \frac{\varepsilon_{c,average} l_g}{n_{cr}} \leq 0.3mm \qquad (23)$$

The number of cracks n_{cr} represents the average number of cracks within the gauge length l_g. The difference between the crack spacing between major cracks and secondary cracks at the reinforcement level is considered using a factor of 0.5, resulting in the relevant number of cracks as determined in Eq. (24):

$$n_{cr} = \frac{l_g}{0.5 l_{cr}} \qquad (24)$$

Resulting Traffic Light System

Table 9 gives an overview of the traffic light system for stop criteria. For reference, the critical locations for measurements in slabs are given in *Fig. 12*. The explanation of the AE-based stop criteria, as included in Table 9, is provided in Ref. [32].

Levels of Information

Proof load testing can be applied to bridges of which various levels of information are available. Ideally, all information about the bridge is available, as detailed information will facilitate the preparations of the load test. *Fig. 13* shows various levels of information that the engineer can encounter regarding an existing bridge that may be subjected to a proof load test.

For the stop criteria, the state of information regarding bridge documentation and material data is relevant. For the shear stop criteria and flexural stop criteria, information about the reinforcement and the concrete compressive strength improves the accuracy of the stop criteria, as this information is relevant for making the sectional analysis. However, when this information is not available, different decisions can be made. In terms of the reinforcement, two options are available: (1) make an educated guess, or (2) carry out a non-destructive test to determine the reinforcement bar diameter and layout. In terms of the concrete compressive strength, three options are available: (1) take information from similar bridge types, which in the Netherlands is catalogized and available[60], (2) use core testing results from a similar bridge built with similar materials in a similar time period, or (3) collect core samples from the bridge to obtain the concrete compressive strength of the structure itself.

When a first guess of the stop criteria needs to be made, and information about the reinforcement and the concrete compressive strength is not available, the following simplifications can be made for reinforced concrete solid slab bridges in the Netherlands, assuming the bridge is built during the peak period of construction from the mid 1960s to mid 1970s:

- $\rho \approx 0.8\%$
- $\varphi \approx 20$ mm
- $f_c \approx 45$ MPa
- $d \approx h - 50$ mm

The general first ballpark value of the reinforcement ratio that is given here corresponds to cases of older bridges, where larger diameters and lower yield strengths of the steel are used (and using a conservative lower bound to derive the stop criteria; many times higher reinforcement percentages are found). In addition, vintage details such as bent up bars and large hooks that may act as local shear reinforcement, will positively influence the shear performance; these are ignored in this simplified, lower-bound proposal.

Discussion

The resulting traffic light system gives a broader tool to the bridge engineer to make decisions during a proof load test. Traditionally, stop criteria have been linked to the elastic response of the structure, and serve to avoid irreversible damage. However, a clear threshold of elastic response cannot always be observed, especially for shear. Therefore, a traffic light system to understand the consequences of further loading the structure has been developed. Two main advances in terms of the theoretical underpinnings of the shear stop can be highlighted. Physical-based models for shear resistance are used to develop theoretically based shear stop criteria for the first time. Using mechanics-based shear models, the possibility of capturing shear failure indicators prior to the brittle shear failure is demonstrated. These advances in the theoretical basis of the stop criteria are unique in the field of bridge load testing, and mark a major step forward. In addition, cross-validation of the proposed approaches with work ongoing in Denmark shows synergy in ideas and applications.[61,62] Active international collaboration on the topic allows for exchange of ideas, insights, and best practices,[63] which facilitates the development of practical guidelines and recommendations.

Three main improvements have been made with this research.

- The uncertainties on the stop criteria have been significantly reduced, with coefficients of variation between 12% and 21% (and one outlier of 29%). These values are encouraging, given that: (1) the considered failure mode is shear, for which the mechanical basis is still subject to discussion, and (2) shear stop criteria aim at capturing effects of shear failure prior to the

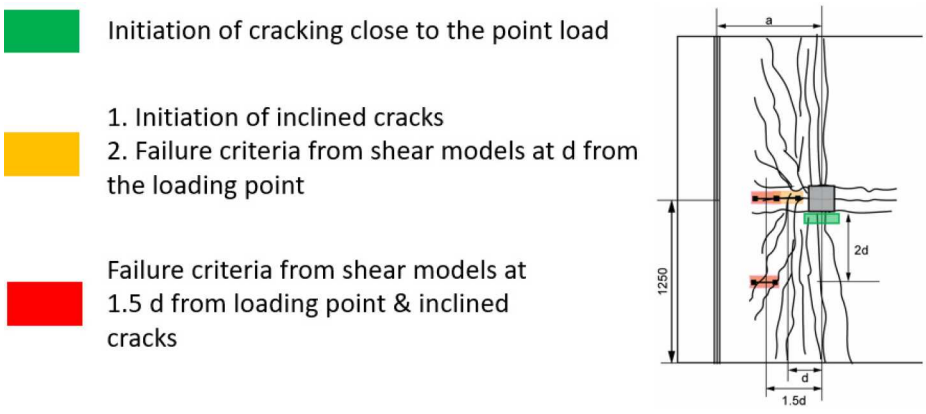

Fig. 12: Traffic light system of stop criteria for slabs

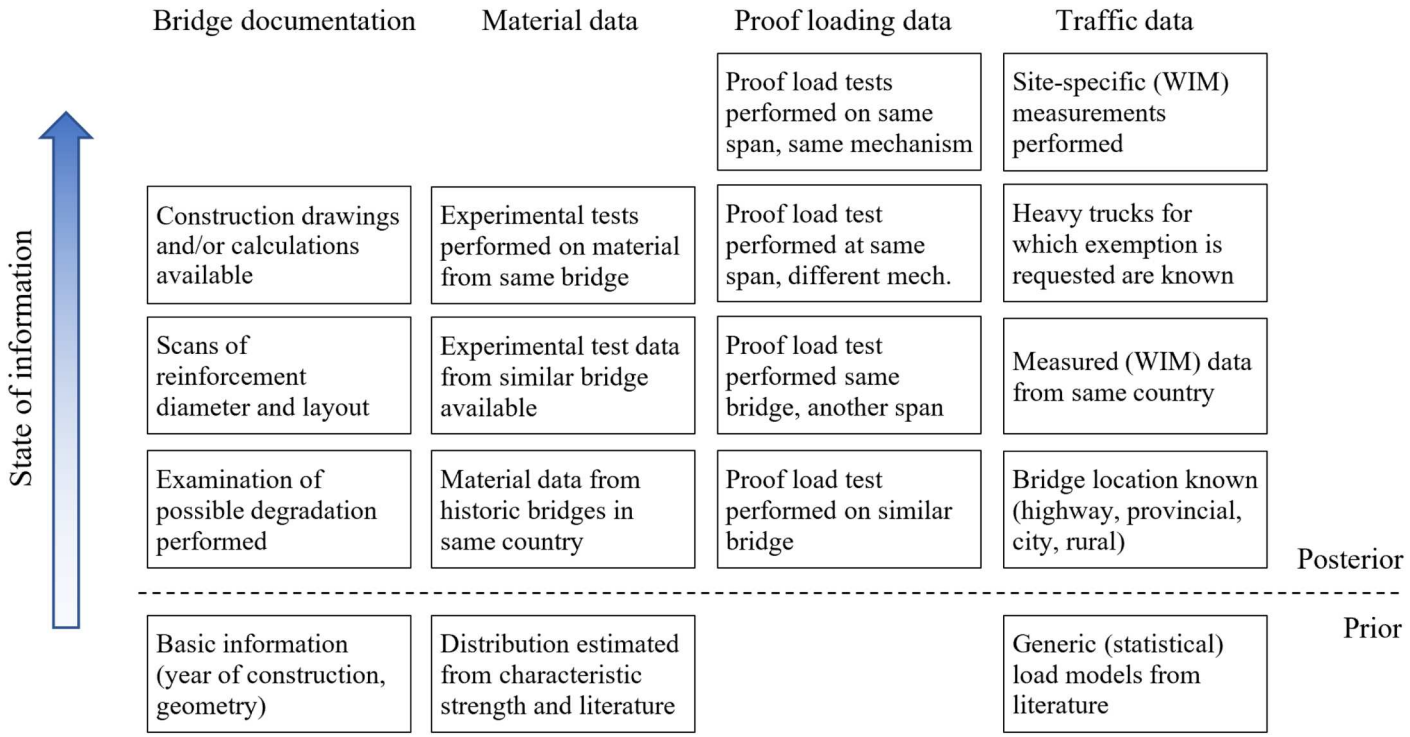

Fig. 13: State of information of existing bridges for proof load testing[59]

failure, further complicating the mechanics at work.

- By moving from stop criteria to a traffic light system of stop criteria, stop criteria are now interpreted in terms of various potential consequences of loading, from green light (potential serviceability issues and remaining cracking), via yellow light (intermediate warning that more attention needs to be paid to the bridge performance at the next load levels), to red light (further loading can result in a local failure). This approach gives us further information during the test, for a modest number of additional measurements.
- The flexural stop criteria[55] have been adapted to the traffic light system, so that the traffic light system encompasses both serviceability, shear, and flexure.

As the current work has only been validated with laboratory experiments, the main limitation is that the traffic light system has not yet been applied during an actual proof load test. In addition, open questions that remain to be addressed theoretically are:

1) the effect of continuity near the support and its effect on the stop criteria and the determination of the critical measurement location,
2) uncertainties introduced in the yellow and red stop criteria related to the associated measurement location using $M/Vd \times 1/\lambda$ (e.g. in continuous members where the moment distribution is not known exactly, or in skewed members),
3) bar curtailments and their effect on the shear capacity and stop criteria via the anchorage length,
4) influence of damage and deterioration on the stop criteria, for example the validity of the shear stop criteria for members with corroded reinforcement,
5) application to special types of concrete, such as lightweight concrete,
6) very skewed members, and
7) effect of strong strips with shear reinforcement at the edges of reinforced concrete slab bridges, which improve the transverse load distribution.

Further integration of nonlinear finite element models or derived surrogate models for the interpretation of the structural responses, can be further explored. The new insights also need to be integrated into the Bayesian framework for determining the structural reliability developed in parallel to this research.[54,59,64] Ultimately, the proposed set of stop criteria need to be validated in the field, ideally with a proof load test followed by a collapse test.

Conclusions

This paper develops a set of stop criteria for shear and flexure for the application in proof load testing of reinforced concrete solid slab bridges without shear reinforcement. This paper provides the following main conclusions:

- Shear stop criteria are derived based on two mechanical models, the Critical Shear Displacement Theory and the Critical Shear Crack Theory. The derivation shows that indicators can be found prior to failure of a brittle shear failure.
- To extend the shear stop criteria to slabs, the waviness of the crack pattern needs to be taken into account and the critical location is linked to $M/Vd \times 1/\lambda$ derived from linear finite element analysis.
- All proposed stop criteria can be organized together in a traffic light system, which gives indications at various levels of loading about the structural performance of the tested bridge.
- The validation of the proposed stop criteria on the three sets of experiments show overall consistent behaviour, except for the skewed slab members where the

measurements were not applied in the correct $M/Vd \times 1/\lambda$ region, as well as an acceptable probability of failure without reaching a stop criterion.

The proposed traffic light system of stop criteria is a step forward in the broader and better-informed application of proof load testing for the assessment of existing concrete bridges. Field validation is necessary as a next step, which then may lead to improved guidelines and recommendations for practice.

List of Notations

a	shear span
b	member width
b_{cr}	the real length of the critical crack in the transverse direction
c	height of the compression zone
d_g	maximum aggregate size
d	effective depth to the longitudinal reinforcement
d_c	cover to the centroid of the tension reinforcement
d_x	the width of the transverse strip of the slab
$d\tilde{x}_{cr}$	the average variation of the transverse crack profile in the longitudinal direction, or the wave amplitude of the crack profile
f_c	concrete compressive strength
$f_{c,cube}$	cube concrete compressive strength
f_{ctm}	mean tensile strength of the concrete
f_{perm}	stress in the steel caused by the permanent loads
f_{ym}	average yield strength of reinforcement steel
f_{um}	average ultimate strength of reinforcement steel
h	height of cross-section
k_w	bedding stiffness
l	length of the slab
l_{cr}	average crack spacing
l_g	gauge length
l_t	the transfer length
l_w	influencing length in a slab
n	ratio between the Young's modulus of the steel and the Young's modulus of the concrete
n_{cr}	average number of cracks within the gauge length
s	reinforcement spacing
s_{cr}	height of a fully developed crack
v_0	magnitude of the principal shear force per unit length of a loaded slab
v_x	unitary shear force in x-direction
v_y	unitary shear force in y-direction
w	nominal crack width at the level of the steel reinforcement
w_{avg}	average crack width
w_{max}	maximum measured crack width during loading
w_{res}	residual crack width after a loading cycle
w_{stop}	crack width flexural stop criterion
x	the distance of a local weak spot to the support
x_{cr}	length of the critical crack from the tip to the root in the longitudinal direction
A_p	amplitude of the transverse crack
E	Young's modulus of the concrete
E_s	modulus of elasticity of reinforcing bars
G	shear modulus of the concrete
I_x	x-direction moment of inertia
I_{CSCT}	shear indicator of the CSCT
I_{CSDT}	shear indicator of the CSDT
$I_{CSDT,cr}$	critical shear indicator using the CSDT
M	sectional moment
M_x	x-direction slab moment
M_{xy}	torsional moment in slabs
M_y	y-direction slab moment
M_1	principal moment in direction 1
P_{cr}	inclined cracking load in experiments
P_{stop}	load at which stop criterion is reached
P_u	maximum load in experiments
T	period of the waveform of the cracking profile
V	sectional shear
V_{ai}	aggregate interlock capacity
V'_{ai}	aggregate interlock capacity in wide members
V_R	shear resistance
α_1	principal direction associated with M_1
β_{fr}	strain gradient factor used in the method of Frosch[56]
ε_c	measured smeared strain on the concrete
ε_{c0}	analytically determined short-term strain in the concrete caused by the permanent loads acting on the structure before the application of the proof load
$\varepsilon_{c,average}$	averaged strain measured over gauge length
$\varepsilon_{c,bot,max}$	concrete strain at the bottom of cross-section that corresponds to a yield stress in the steel of the yield strength
ε_{stop}	strain limit flexural stop criterion
ε_x	longitudinal strain
$\varepsilon_{x,rebar}$	longitudinal strain at the level of the reinforcement
φ	the reinforcement diameter
φ_o	direction of the principal shear force
ϕ_{eq}	equivalent rebar diameter
ϕ_i	rebar diameter of the i-th bar
θ	rotation
λ	$= a/d$; a factor to account for shear slenderness in which the shear stop criteria are reached first
ν	Poisson ratio
ρ_{eff}	the effective reinforcement ratio
ρ_l	reinforcement ratio of the longitudinal reinforcement
τ	acting shear stress at the cracked section
τ_{bm}	average bond between reinforcement and concrete
Δ	shear displacement
Δ'	shear displacement in wide members
Δ_{cr}	critical shear displacement as used in the Critical Shear Displacement Theory
Ψ_s	multiplication factor

Disclosure Statement

No potential conflict of interest was reported by the author(s).

Funding

This work was supported by Rijkswaterstaat.

Data Availability Statement

The data is available upon request.

References

[1] Cervantes E, Flores K, Lantsoght E, Matos JC. UAV-Visual Inspection: bridge condition assessment over a decade. *IABSE Congress 2024: Beyond Structural Engineering in a Changing World*: IABSE; 2024. p. 1298-1306.

[2] Lantsoght E, Yang Y, Hendriks M, editors. Extending the service life of existing concrete bridges using improved assessment methods. *IABSE Congress 2024: Beyond Structural Engineering in a Changing World*: IABSE; 2024.

[3] Lantsoght EO. Assessment of existing concrete bridges by load testing: barriers to code implementation and proposed solutions. Struct Infrastruct Eng. 2023: 1–13.

[4] Bagge N. *Structural Assessment Procedures for Existing Concrete Bridges: Experiences from Failure Tests of the Kiruna Bridge*. Lulea: Lulea University of Technology, 2017.

[5] Bertola NJ, Henriques G, Brühwiler E. Assessment of the information gain of several monitoring techniques for bridge structural examination. J Civil Struct Health Monit. 2023. doi:10.1007/s13349-023-00685-6

[6] Cosenza E, Losanno D. Assessment of existing reinforced-concrete bridges under road-traffic loads according to the new Italian guidelines. Struct Concrete. 2021; 22(5): 2868–2881. doi:10.1002/suco.202100147

[7] Decò A, Frangopol DM. Risk assessment of highway bridges under multiple hazards. J Risk Res. 2011; 14(9): 1057–1089. doi:10.1080/13669877.2011.571789

[8] Ferreira D, Marí A, Bairán J. Assessment of prestressed concrete bridge girders with low shear reinforcement by means of a non-linear

filament frame model. Struct Infrastruct Eng. 2014; 10(12): 1531–1546. doi:10.1080/15732479.2013.834944

[9] Gara F, Carbonari S, Nicoletti V, Martini R, Brunetti A, Dall'Asta A, et al. Assessment and management of existing bridges following the innovative Italian guidelines: A pilot study. Intern J Bridge Eng Manage Res. 2025; 2(1): 1–18. doi:10.70465/ber.v2i1.19

[10] Gleich P, Maurer R. Bridge reassessment in Germany: shear capacity computation based on arch action model. Proc Inst Civil Eng Eng Hist Herit. 2017; 170(3): 112–124. doi:10.1680/jenhh.16.00024

[11] Grieco LA, Scattarreggia N, Monteiro R, Parisi F. An index-based multi-hazard risk assessment method for prioritisation of existing bridge portfolios. Intern J Disaster Risk Reduct. 2024; 114: 104895. doi:10.1016/j.ijdrr.2024.104895

[12] Mandić Ivanković A, Hrelja Kovačević G, Vlašić A, Srbić M, Skokandić D. Seismic assessment of existing bridges: shortcomings vs hidden reserves. Beyond Struct Eng Chang World. 2024: 192–200.

[13] Muttoni A, Ruiz MF. Levels-of-Approximation approach in codes of practice. Struct Eng Intern. 2012; 22(2): 190–194. doi:10.2749/101686612X13291382990688

[14] Šavor Z, Šavor Novak M. Procedures for reliability assessment of existing bridge. Građevinar. 2015; 67(6): 557–572.

[15] Valenzuela M. The case study of Chile—how quality control could improve better life-cycle management of bridges. *Life Cycle Analysis and Assessment in Civil Engineering: Towards an Integrated Vision*: CRC Press; 2018. p. 1811-1818.

[16] fib. *Model Code 2010: Final Draft*. Lausanne: International Federation for Structural Concrete, 2012. 676.

[17] Belletti B, Damoni C, den Uijl JA, Hendriks MAN, Walraven JC. Shear resistance evaluation of prestressed concrete bridge beams: fib model code 2010 guidelines for level IV approximations. Struct Concrete. 2013; 14(3): 242–249. doi:10.1002/suco.201200046

[18] Belletti B, Pimentel M, Scolari M, Walraven JC. Safety assessment of punching shear failure according to the level of approximation approach. Struct Concrete. 2015; 16(3): 366–380. doi:10.1002/suco.201500015

[19] Lantsoght EOL, De Boer A, Van der Veen C. Levels of approximation for the shear assessment of reinforced concrete slab bridges. Struct Concrete. 2017; 18: 143–152. doi:10.1002/suco.201600012

[20] Deutscher Ausschuss für Stahlbeton. *DAfStb-Richtlinie: Belastungsversuche an Betonbauwerken*. Jui: Deutscher Ausschuss fur Stahlbeton, 2020.

[21] ACI Committee 437. Code Requirements for Load Testing of Existing Concrete Structures (ACI 437.2-22) and Commentary Farmington Hills, MA; 2022.

[22] Lantsoght EOL, Yang Y, Tersteeg RHD, van der Veen C, de Boer A. *Development of Stop Criteria for Proof Loading*. Delft: IALCCE, 2016, 8.

[23] Rodriguez A, Lantsoght EOL. *Verification of Flexural Stop Criteria for Proof Load Tests on Concrete Bridges Based on Beam Experiments*. Ghent: IALCCE, 2018.

[24] Lantsoght EOL, Yang Y, van der Veen C, Hordijk DA. *Stop Criteria for Proof Load Tests Verified with Field and Laboratory Testing of the Ruytenschildt Bridge*. Copenhagen: IABSE, 2018.

[25] ACI Committee 437. Code Requirements for Load Testing of Existing Concrete Structures (ACI 437.2M-13) and Commentary Farmington Hills, MA; 2013.

[26] Koekkoek RT, Yang Y. *Measurement Report on the Transition Between Flexural and Shear Failure of RC Beams Without Shear Reinforcement*. Delft University of Technology, 2016.

[27] Yang Y, van der Ham H, Naaktgeboren M. Shear Capacity of RC Slab Structures with Low Reinforcement Ratio - an Experimental Approach. fib symposium 2021; Lisbon (online)2021.

[28] MatchID. User manual. 2022.

[29] The Mathworks I. Matlab R2019a, User's Guide. Natick, USA2019.

[30] Gehri N, Mata-Falcón J, Kaufmann W. Automated crack detection and measurement based on digital image correlation. Construct Build Mater. 2020; 256: 119383. doi:10.1016/j.conbuildmat.2020.119383

[31] Zarate Garnica G, Lu J, Yang Y, Hendriks MAN, Lantsoght EOL. Shear experiments On straight reinforced concrete slabs. Proc Intern Struct Eng Construct. 2024; 11(1): 1.

[32] Zhang F. *Acoustic Emission-Based Indicators of Shear Failure of Reinforced Concrete Structures Without Shear Reinforcement*. Delft University of Technology, 2022.

[33] Zarate Garnica GI, Lantsoght EOL. *Measurement Report of Reinforced Concrete Slabs*. Delft: Delft University of Technology, 2021.

[34] Zarate Garnica GI, Lantsoght EOL, Yang Y, Hendriks MAN. Capacity of reinforced concrete one-way slabs under concentrated loads. ACI Structural Journal. 2026;available ahead of print.

[35] Lu J, Yang Y, Lantsoght E. Preparation report for skewed slab test. Delft, the Netherlands; 2022.

[36] Lu J, Yang Y, Lantsoght E. Measurement report for skewed slab test: Part I & Part II. Delft, the Netherlands; 2024.

[37] Lantsoght EOL, van der Veen C, Walraven JC, de Boer A. Case study on aggregate interlock capacity for the shear assessment of cracked reinforced-concrete bridge cross sections. J Bridge Eng. 2016; 21(5): 04016004-1–04016004-10. doi:10.1061/(ASCE)BE.1943-5592.0000847

[38] Sherwood EG, Lubell AS, Bentz EC, Collins MP. One-way shear strength of thick slabs and wide beams - authors' closure. Aci Struct J. 2007; 104(5): 640–641.

[39] Sherwood EG, Bentz EC, Collins MR. Effect of aggregate size on beam-shear strength of thick slabs. Aci Struct J. 2007; 104(2): 180–190.

[40] Swamy RN, Andriopoulos AD, editors. Contribution of aggregate interlock and dowel forces to the shear resistance of reinforced beams with Web reinforcement. *ACI Symposium March and October 1973*. American Concrete Institute; 1973.

[41] Yang Y, Walraven J, den Uijl JA. Shear behavior of reinforced concrete beams without transverse reinforcement based on critical shear displacement. J Struct Eng. 2017; 143(1): 04016146-1–04016146-13. doi:10.1061/(ASCE)ST.1943-541X.0001608

[42] Yang Y, Den Uijl JA, Walraven J. The critical shear displacement theory: on the way to extending the scope of shear design and assessment for members without shear reinforcement. Structu Concrete. 2016; 17(5): 790–798. doi:10.1002/suco.201500135

[43] Yang Y, Zárate Garnica G, Lantsoght EOL, Hordijk DA. Calibration of the shear stop criteria based on crack kinematics of reinforced concrete beams without shear reinforcement. fib conference 2018; Melbourne, Australia2018.

[44] Muttoni A, Ruiz MF. Shear strength of members without transverse reinforcement as function of critical shear crack width. Aci Struct J. 2008; 105(2): 163–172.

[45] Lantsoght EOL, Yang Y, van der Veen C, de Boer A, Hordijk DA. Beam experiments on acceptance criteria for bridge load tests. ACI Struct J. 2017; 114(4): 1031–1041.

[46] Zarate Garnica GI, de Vries R, Lantsoght EOL. *Analysis Report of Reinforced Concrete Slabs for Stop Criteria*. Delft University of Technology, 2022.

[47] Zarate Garnica GI, Lantsoght EOL, Yang Y, Hendriks MAN. Shear stop criteria for reinforced concrete slab strips. IABMAS; 20242024.

[48] Yang Y. *Shear Behaviour of Reinforced Concrete Members Without Shear Reinforcement: A New Look at an Old Problem*. Delft University of Technology, 2014.

[49] Marti P. Design of concrete slabs for transverse-shear. Aci Struct J. 1990; 87(2): 180–190.

[50] Natário F, Ruiz MF, Muttoni A. Shear strength of RC slabs under concentrated loads near clamped linear supports. Eng Struct. 2014; 76: 10–23. doi:10.1016/j.engstruct.2014.06.036

[51] Zarate Garnica GI. *Shear Stop Criteria for Proof Loading of Reinforced Concrete Slab Bridges*. Delft University of Technology, forthcoming.

[52] Lu J, Lantsoght EOL, Yang Y. Preparation report for skewed slab test. Stevin II report. 2022 (25.5-22-08).

[53] Lantsoght EOL, Zarate Garnica GI, Yang Y, Hendriks MAN. *Development and Validation of Shear Stop Criteria for Proof Load Testing of RC Slab Bridges*. Delft University of Technology, 2024.

[54] de Vries R, Lantsoght EOL, Steenbergen RDJM, Hendriks MAN, Naaktgeboren M. Structural reliability updating on the basis of proof load testing and monitoring data. Eng

Struct. 2025; 330: 119863. doi:10.1016/j.engstruct.2025.119863

[55] Lantsoght EOL, Yang Y, van der Veen C, Hordijk DA, de Boer A. Stop criteria for flexure for proof load testing of reinforced concrete structures. Front Built Environ. 2019; 5(47. doi:10.3389/fbuil.2019.00047

[56] Frosch RJ. Another look at cracking and crack control in reinforced concrete. ACI Struct J. 1999; 96(3.

[57] Deutscher Ausschuss für Stahlbeton. *DAfStb-Richtlinie: Belastungsversuche an Betonbauwerken*. Deutscher Ausschuss fur Stahlbeton, 2000.

[58] Lantsoght E, Yang Y, van der Veen C, de Boer A, Hordijk D. Ruytenschildt bridge: field and laboratory testing. Eng Struct. 2016; 128(december): 111–123. doi:10.1016/j.engstruct.2016.09.029

[59] de Vries R, Lantsoght EOL, Steenbergen RDJM, Fennis SAAM. Reliability assessment of existing reinforced concrete bridges and viaducts through proof load testing. IABMAS 2022; Barcelona, Spain 2022.

[60] Vervuurt A, Courage W, Steenbergen R. Betonsterkte bestaande constructies. Cement. 2012; 64(4): 36–39.

[61] Schmidt JW, Christensen CO, Damsgaard K, Lantsoght EOL, Yang Y, Goltermann P. Validation of proof loading methods: With a basis in collapse testing and stop criteria evaluation. IABSE Congress Ghent 2025 – The Essence of Structural Engineering for Society; Ghent, Belgium2025.

[62] Schmidt JW, Christensen CO, Damsgaard K, Lantsoght EOL, Yang Y, Goltermann P. In-situ and laboratory collapse testing in a proof loading perspective. IABSE Congress Ghent 2025 – The Essence of Structural Engineering for Society; Ghent, Belgium2025.

[63] Bertola N, Bhowmick A, Casas JR, Chacon R, Cousins D, Grimson J, et al. Bridge Load Testing for Assessment: Recent Advances in Application, Collaboration, Codes, and Research. Structure and Infrastructure Engineering. in press.

[64] de Vries R, Lantsoght EOL, Steenbergen RDJM, Fennis SAAM. Time-dependent reliability assessment of existing concrete bridges with varying knowledge levels by proof load testing. Struct Infrastruct Eng. 2023: 1–15.